

# Gas forming of an AZ31 magnesium alloy at elevated strain rates

D. Sorgente<sup>1</sup> · G. Palumbo<sup>1</sup> · L. D. Scintilla<sup>1</sup> · L. Tricarico<sup>1</sup>

Received: 22 May 2015 / Accepted: 19 July 2015 / Published online: 1 August 2015  
© Springer-Verlag London 2015

**Abstract** In this work, the gas forming of AZ31 magnesium alloy 0.75-mm-thick sheets at elevated strain rates (fast gas forming) is investigated through an experimental-numerical approach. First, free inflation tests were carried out to find the conditions, in terms of temperature and forming pressure, able to give the best compromise between the alloy formability and the forming time. The analysis was successively moved to a closed die forming application with a stepped geometry case study in order to analyse the real forming process. Both an axisymmetric model of the free inflation test and a 3D model of the closed die forming process were built to correlate the results from free inflation tests (in terms of optimal strain rate values) to the closed die forming test: Numerical simulations were run to find the pressure value to be applied in gas forming tests. Experimental gas forming trials were finally conducted in order to support the approach and to analyse post-forming characteristics of the formed parts. Results showed that very small fillet radii can be reached on a commercial Mg alloy sheet setting very short forming times (few seconds). The choice of the forming temperature and of the corresponding optimal strain rate strongly affects the grain growth and the cavitation phenomena. Even if the alloy is prone to a strong static and dynamic grain growth at elevated temperatures, a small mean grain size value can be reached in the formed component due to the short forming times.

**Keywords** Magnesium alloy · Gas forming · Superplastic forming · FE model

## 1 Introduction

In recent years, the word “fast”, as well as “rapid” or “quick”, for the gas forming process is spreading out with the meaning of a superplastic-like gas forming process in which cycle times are significantly shorter than conventional superplastic forming. Neugebauer et al. provided a net distinction between superplastic forming and fast gas forming based on the cycle time, that ranges from minutes to hours in the former while it has a duration of few seconds in the latter [1]. In the fast gas forming process, the forming technique is the same of the conventional superplastic forming one: It is based on the blow forming approach, which adopt a relatively low gas pressure as forming tool acting on a thin heated metal sheet that expands (with negligible drawing) in a female die. By the combination of the potentialities of this approach with wrought materials, such as magnesium (Mg) alloys, that cannot be successfully formed in complex shapes at room temperature, great interest arises towards such a process in several industrial fields [2]. Deformation mechanisms in the two process families (superplastic forming and fast gas forming) are obviously different. Recent studies demonstrated that large elongations to failure can be reached in wrought Mg alloys even if the grain boundary sliding (GBS) is not main deformation mechanism [3]. In mass production, the superplastic forming has not a large-scale application. This is mainly due to the high cost of the process and to its characteristic large cycle time, which make this process globally less competitive than other conventional ones. In order to overcome these limits, high strain rate superplasticity as well as techniques as the quick plastic forming have been developed and are continuously

---

✉ D. Sorgente  
d.sorgente@poliba.it

<sup>1</sup> Dipartimento di Meccanica, Matematica e Management, Politecnico di Bari, Viale Japigia 182, 70126 Bari, Italy

improving in order to achieve high volume production [4]. It has been also demonstrated that the pressure profile can be improved to speed up the gas forming process on AZ series Mg alloys [5]. Zhang et al. studied the superplastic behaviour of an AZ31 Mg alloy prepared by friction stir processing, and they found elongations to failure above 200 % at 673 and 723 K also with a strain rate of  $10^{-2} \text{ s}^{-1}$  [6]. They also found that grain growth and cavities coalescence play important roles in the deformation behaviour of the AZ31 Mg alloy at 673 and 723 K, while dynamic recrystallisation dominates the structure evolution at 573 K. Chung et al. investigated the superplastic behaviour of a fine-grained AZ61 Mg alloy sheet during equi-biaxial tensile deformation: Thin circular diaphragms (0.7 mm in thickness) were successfully deformed into hemispherical domes at 673 K applying gas pressures in the range 0.46–1.20 MPa. They concluded that, adopting high pressure levels (0.8 and 1.2 MPa), the creep deformation mechanism for the Mg alloys changes from the lattice diffusion (DL) controlled GBS to the DL-controlled dislocation climb due to dynamic grain growth occurring during the forming process [7]. Wu et al. have successfully formed a fine-grained AZ31B-O Mg alloy at 693 K into a shallow rectangular pan characterised by a width to depth ratio of 5 and by a fillet radius smaller than 2 mm. Such results were achieved by constant gas pressure blow forming tests, setting a cycle time shorter than 2 min. They stated that the dislocation creep is the predominant deformation mechanism at strain rates approximately in the order of  $10^{-2} \text{ s}^{-1}$  and at the temperature of 693 K [8]. Moreover, the fine-grained structure seems not to be a fundamental requirement if high elongations to failure have to be reached. In fact, El-Morsy et al. reported a superplastic behaviour of an AZ31 Mg alloy even if it had an initial relative coarse grain structure. They measured, through the multi-dome test conducted at 673 K, a strain rate sensitivity index ( $m$ ) of 0.45 and a strain rate value of about  $5 \times 10^{-4} \text{ s}^{-1}$  [9]. Moreover, as reported by Kim et al., at elevated temperatures, the grain coarsening of the AZ31 Mg alloy is so significant that a comparison between alloys with different initial grain sizes can be vane: The extremely fast grain growth makes the alloys similar from the microstructural point of view after short testing times. This is due to the dissolution of the  $\text{Mg}_{17}\text{Al}_{12}$  phase particles into the Mg matrix above 473 K [10].

The principal issues to be handled during the deformation of Mg alloys, especially at elevated temperature and for large strain to be reached, are the cavitation, the grain growth and also the interaction between the above-mentioned phenomena. According to Lee and Huang, the major factors affecting the cavitation behaviour are the loading temperature, the strain rate, the strain level and the mean grain size [11]. As for the grain growth, the static and the dynamic components can be assumed to contribute independently, and hence, their coupling gives the total grain growth. Several predictive models

exist for both the static and the dynamic grain growth of several alloys. Among them, the model developed by Miao et al. for a hot-rolled AZ31 Mg alloy can be assumed for predicting the static growth in the range of 523–723 K and for annealing times up to 120 min [12]. This model highlights that the annealing temperature effect on grain size is more significant than the annealing time one. Thus, reducing the forming temperature is not only beneficial for its intrinsic economic advantage but also because it provides better post-forming characteristics in terms of final grain size. Sorgente et al. analysed the forming behaviour of a commercial AZ31 Mg alloy sheet at elevated temperature both in free bulging and in closed die tests. Results from experimental activities highlighted that the die filling increases more than linearly according to pressure and less than linearly according to forming time. Moreover, in the explored temperature range, a good compromise between elongation to failure, strain rate sensitivity index and material post-forming conditions can be achieved at 733 K [13]. Among above-mentioned works, the definition of the optimal value of the forming temperature is controversial: Some authors claim that working at 673 K is more appropriate for the AZ31 alloy due to the strong temperature influence on the grain growth, while other authors prefer to work at 723 K because the elongations to failure which can be reached are higher and, at the same time, the forming time can be drastically reduced [3, 9, 14, 15]. A drawback of operating at high temperature is the orange-peel surface that can be observed on the formed part, especially when low strain rate values are adopted [16].

The aim of this work is to demonstrate the potentialities of the fast gas forming process to manufacture complex shape components using an AZ31 Mg alloy. The experimental campaign, conducted in the temperature range 623–723 K setting high forming pressure levels, was aimed at investigating the behaviour of such Mg alloy at high strain rates. After detailing and discussing the results of the experimental campaign, a deeper insight of the fast gas forming process of the AZ31 Mg alloy is given and suitable process parameters are provided. The work consists of two parts: The first part is focused on the material characterisation; the second part concerns the fast gas forming process analysis. In the first part, the material ability to reach elevated elongations to failure was evaluated measuring the final dome height at failure reached in free inflation tests. Apart from a marked superplastic behaviour at low forming pressure values, a process window characterised by good formability at high pressure values was found taking into account also the microstructural evolution of the alloy. In the second part, a numerical model of the fast gas forming process of a stepped geometry case study was built to define the optimal forming pressure value. Experimental closed die forming tests were finally carried out to validate the results from both the characterisation and the numerical analysis.

## 2 Material and methods

### 2.1 Material and metallographic analysis

A single batch of AZ31B (MgAl3Zn1 wt%) sheets having an average grain size of  $11.0 \pm 0.4 \mu\text{m}$  and a thickness of  $0.75 \pm 0.07 \text{ mm}$  was purchased in the annealed condition. Grain boundaries were revealed by chemical etching after mechanical polishing both on the as-received material and on the deformed specimens. For this purpose, the acetic picral solution containing 4.2 g picric acid, 10 ml acetic acid, 10 ml  $\text{H}_2\text{O}$  and 70 ml ethanol was used. Optical microscopy observations were conducted using an inverted microscope (NIKON MA200). In Fig. 1, the microstructure of the as-received sheet is reported.

The microstructure of the as-received alloy is characterised by fine and equiaxed grains typical of a completely annealed and recrystallised material structure.

### 2.2 Free inflation tests for the material characterisation

The material characterisation through free inflation tests was performed on the laboratory scale equipment embedded in the cylindrical split furnace of an INSTRON 4485 universal testing machine. The equipment is composed of (i) a blank holder; (ii) a female die (having a 45-mm diameter and an entry radius of 3 mm); (iii) a pneumatic circuit for the gas supply, in turn, composed of an argon cylinder, proportional electronic valves, steel tubes in the proximity of the forming chamber and flexible polyurethane tubes in colder zones; (iv) an INSTRON electric furnace characterised by three independent heated and controlled zones (the upper, the central and the lower), which was set to three different temperature levels in order to compensate the thermal dispersion; (v) thermocouples to monitor the thermal condition on the sheet and on the tools; (vi) a transducer for measuring the specimen dome height during the bulging test and (vii) a PC equipped with a data acquisition I/O device by which the test parameters (pressure, temperature and also blank holder force) could be

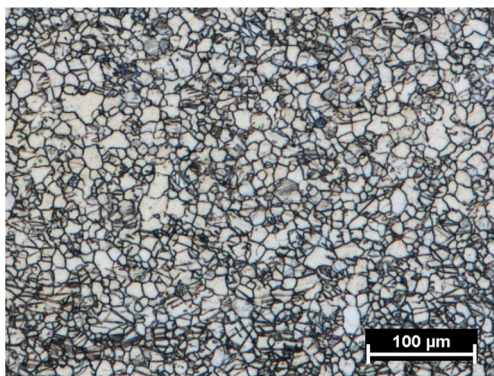


**Fig. 1** The microstructure of the AZ31 Mg alloy in the as-received condition

monitored and managed. A schematic representation of the test is given in Fig. 2: The sheet can freely expand in the cylindrical die cavity. Further details can be found in [17].

The blank is not preheated, and it is interposed between the die and the blank holder when they have reached the test temperature. Due to its small thickness and, consequently, to its small thermal capacity, the sheet reaches a stable test temperature in about 100 s. To limit the effect of the static grain growth during the test and to assure a uniform temperature across the sheet, each test was started, i.e. the gas pressure was raised up to the test value, 120 s after positioning the blank between the tools and setting the blank holder force. Even if the duration of the phase before the gas inflation is comparable to one of the forming test, the static grain growth in such a transient phase was considered negligible since the temperature is in a rising phase.

### 2.3 Forming tests and case study

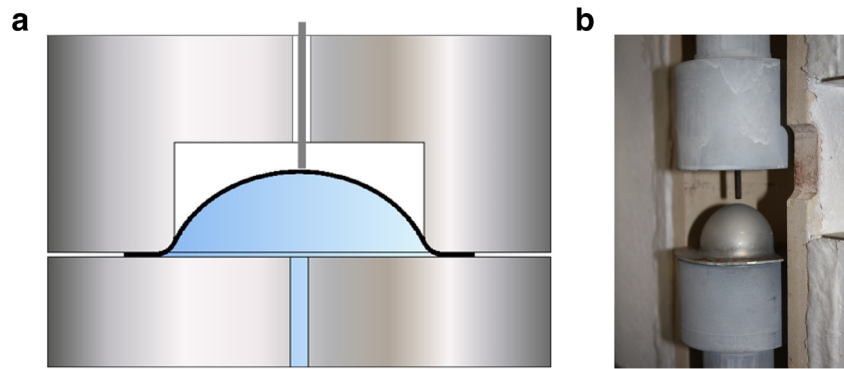
Gas forming tests were carried out using the equipment shown in Fig. 3. In particular, the 2500 kN electro-hydraulic press machine (four electric motors supported by additional two hydraulic cylinders for increasing the closing force), specifically designed in collaboration with the Gigant Italia company, was used.

The press machine is suitable for both warm hydroforming and superplastic forming tests, being equipped with heated tools for warm (up to 623 K) and hot conditions (up to 1273 K). In the present work, for the fast gas forming tests, the hot working tools were used. In particular, the lower tool contains a metallic blank holder, while the upper tool contains a fibre reinforced refractory castable (FRRC) insert as a die, whose geometry is also reported in Fig. 3: It is a stepped shape characterised by a two depths die cavity, respectively equal to 12 and 20 mm.

Each tool (both the lower and the upper one) contains a Nichel Alloy 600 element embedding six electric cartridges (total power per tool 13.2 kW) managed by the programmable logic control (PLC) of the press machine using temperature data from thermocouples. The thermocouples are placed near the electric cartridges and also in proximity of both the die surface (upper tool) and the blank holder (lower tool). When the temperature difference between the die cavity and the blank holder is smaller than a prescribed value, the heating phase ends and the forming gas is blown into the tools. In the experiments described in this work, a 5 K temperature difference value was set, thus assuring a uniform temperature distribution.

The blank to be formed is introduced into the tools (between the FRRC die and the blank holder) after they have reached the test temperature. Boron nitride is applied to the blank upper surface which is going to be in contact with the FRRC die.

**Fig. 2** Equipment for blow forming tests: **a** schematic drawing of the inflation system and **b** image of the deformed specimen after the free inflation test



The forming gas is blown through the blank holder, and it is not heated due to its negligible thermal capacity. The pressure of the gas is controlled through a proportional electronic valve which is also managed by the PLC in order to obtain any pressure profile defined by the user. In the experiments detailed in the present work, a constant forming pressure level was used. The forming pressure was calculated by means of preliminary finite element (FE) simulations based on the outcomes of the material characterisation (by free inflation tests) in order to subject the blank to an average strain rate close to the optimal value.

#### 2.4 Numerical modelling

Both an axisymmetric and a 3D model were built to analyse the forming process using the commercial FE code ABAQUS/Standard and an elastic-viscoplastic integration.

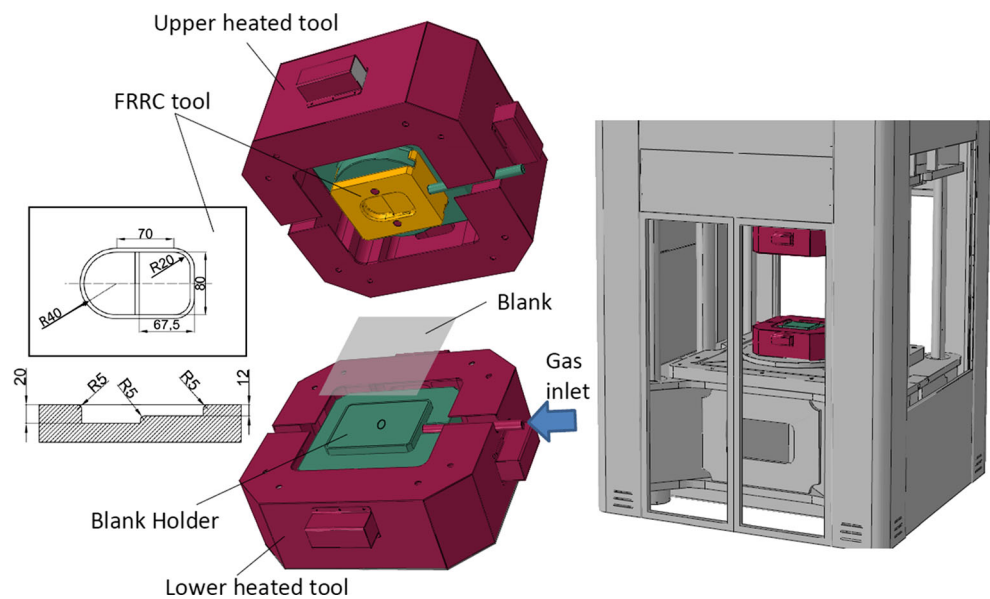
The axisymmetric model reproduced the free inflation test: The Mg alloy deformable blank was divided into 800 continuum elements with four nodes and one integration point; the die was modelled as an analytical rigid surface, and the blank

holder was not modelled. The blank was constrained along its periphery in order to have no translations in the radial direction and to allow only thickness variations.

The 3D model was built to simulate the gas forming process in the closed die characterised by the case study geometry (see Sect. 2.3). Due to the symmetry of the load and of the boundary conditions, only a half of both the blank and the die were modelled in order to reduce computational costs (Fig. 4).

The blank was modelled using 15,000 linear quadrilateral elements (type S4 in the software library, ABAQUS [18]) and the die using 3320 linear triangular and quadrilateral elements (type R3D4 and R3D3 in the software library, respectively, ABAQUS [18]). The tangential behaviour of the contact pair blank/die was modelled setting the Coulomb friction coefficient to 0.15. Since boron nitride was used during the forming tests, this value was chosen according to the results reported by Hanna [19]. Both in the axisymmetric and in the 3D model, a constant pressure was applied. The forming pressure was modelled in order to reproduce the experimental pneumatic inertia measured in the experimental equipment when increasing the pressure up to the maximum value using a linear ramp.

**Fig. 3** Equipment for gas forming tests





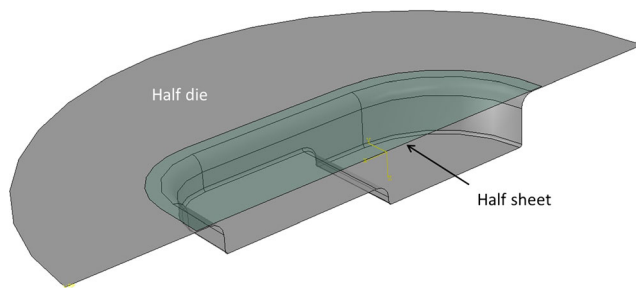


**Fig. 4** Numerical model of the gas forming process

The time to reach the maximum value of the pressure was set to 0.6 and 5 s in the axisymmetric model and in the 3D one, respectively, according to the different pneumatic inertias of the two forming setups (this difference is mainly related to the different volume to be filled in by the gas).

A constant pressure induces a not constant strain rate along the sheet, and the mean equivalent strain rate value  $\bar{\dot{\epsilon}}$  can be calculated as follows:

$$\bar{\dot{\epsilon}} = \frac{1}{t_f} \int_0^{t_f} \dot{\epsilon}(t) dt \approx \frac{1}{t_f} \sum_{t=0}^{t=t_f} \dot{\epsilon}(t) \Delta t \tag{1}$$

where  $t_f$  is the forming time to reach a specific strain,  $\dot{\epsilon}(t)$  is the equivalent strain at time  $t$ ,  $dt$  and  $\Delta t$  are the infinitesimal and the finite time intervals, respectively. The heat transfer was not modelled since the temperature distribution was considered perfectly stable and uniform. The material behaviour at 723 K was modelled according to the equation developed by Carpenter et al. [20]:

$$\dot{\epsilon} = \frac{A_{GBS}}{d^p} \sigma^{n_{GBS}} + A_{DC} \sigma^{n_{DC}} \tag{2}$$

where  $\dot{\epsilon}$  is the equivalent creep strain rate,  $d$  is the mean grain size,  $\sigma$  is the equivalent flow stress,  $A_{GBS}$  and  $n_{GBS}$  are material constants for GBS creep, and  $A_{DC}$  and  $n_{DC}$  are material constants for DC creep.

The mean grain size ( $d$ ) is calculated taking into account both the static and the dynamic growth implementing, by a solution-dependent variable in the numerical model, the equation by Sato et al. [21]:

$$d = d_s e^{\alpha \epsilon} \tag{3}$$

where  $\epsilon$  is the equivalent creep strain,  $\alpha$  is a material constant for the dynamic growth and  $d_s$  is the grain size after the static growth and is calculated as follows:

$$d_s = (d_0^N + Ct)^{1/N} \tag{4}$$

being  $d_0$  is the initial mean grain size,  $t$  is the dwell time,  $C$  and  $N$  are material constants for the static grain growth. Even if the pressure was experimentally raised after the temperature homogenisation, the value of  $d_0$  was set to the initial one since

the static grain growth was neglected (see Sect. 2.2). At each time instant of the simulation, the value of the grain size after static growth is calculated and its value put in Eq. (3) to calculate the grain size value given by both static and dynamic growths. All material constants were set using results by Carpenter et al. [20]. Values of material constants are reported in Table 1. Both planar and normal anisotropies were neglected.

### 3 Material characterisation by free inflation tests

#### 3.1 Free inflation tests

In Fig. 5, results obtained by free inflation tests conducted in the present work are presented together with results from a previous work by the authors [13], in which a lower pressure range was explored on the same alloy.

It can be seen that the highest dome height at failure can be achieved when the pressure level (i.e. the strain rate) is the lowest and the temperature is the highest. This combination of high temperature and low strain rate leads to a superplastic behaviour of the alloy, characterised by a very large elongation to failure. When the temperature decreases, the dome height at failure also decreases and the lowest value of this parameter (measuring the formability of the alloy) can be observed at the lowest temperature (623 K) and the highest pressure (1.50 MPa). At the highest temperature, also the highest pressure sensitivity can be found: A small increase of the forming pressure (0.10–0.20 MPa) at the highest temperature (793 K) leads to a sudden drop of the dome height at failure. On the contrary, at intermediate temperatures (673–723 K), a plateau at around 1.00 MPa can be distinguished, in which the pressure sensitivity is very low and the material exhibits a good formability.

When complex shapes have to be formed, different areas of the sheet undergo to very different stress states and consequently to different strain and strain rate histories: Pressure sensitivity should be as low as possible in order to have a

**Table 1** Material constants used in the equation by Carpenter et al. [20]

Parameter	Value
$d_0$ ( $\mu\text{m}$ )	11
$C$ ( $\mu\text{m s}^{-N}$ )	$1.1 \times 10^{20}$
$N$	22
$a$	0.54
$A_{GBS}$ ( $\text{s}^{-1} \text{MPa}^{-n_{GBS}} \mu\text{m}^p$ )	0.048
$n_{GBS}$	1.3
$P$	3.1
$A_{DC}$ ( $\text{s}^{-1} \text{MPa}^{-n_{DC}}$ )	$3.1 \times 10^{-10}$
$n_{DC}$	5.7

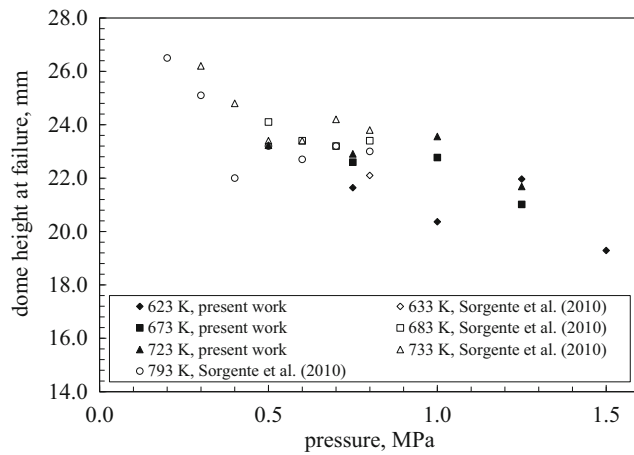


**Fig. 5** Dome height at failure at various temperature and pressure levels

uniform strain behaviour avoiding the occurrence of local critical conditions. This suggests that, when extremely high elongations are not necessary, the forming pressure can be increased since the dome height to failure does not decrease too much in spite of a significant time reduction.

In Table 2, the values of the average time needed to achieve the dome height at failure for different temperature and pressure values are reported.

Working at 673 K, an increase of the pressure from 0.75 to 1.00 MPa leads to a similar dome height at failure, but with a 62 % time reduction; at 723 K, if the pressure is raised from 0.50 to 1.00 MPa, the forming time can be reduced up to 89 % without a significant loss in terms of material formability.

### 3.2 Microstructural evolution

In Table 3, the micrographs of the specimens deformed at 673 and 723 K, both using a gas pressure of 1.00 MPa, are reported. It can be seen that, for both the specimens, in the underformed area (the flange region, between the die and the blankholder) where only the static grain growth occurred, the

mean grain size is very close to the one of the material in the as-received condition ( $11.0 \pm 0.4 \mu\text{m}$ ). On the other hand, the grain size significantly increased in the most deformed areas.

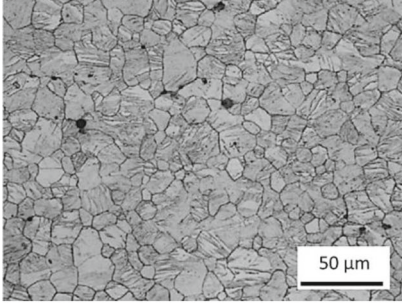
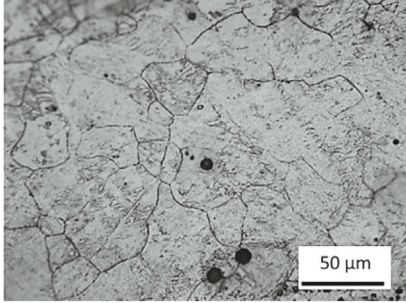
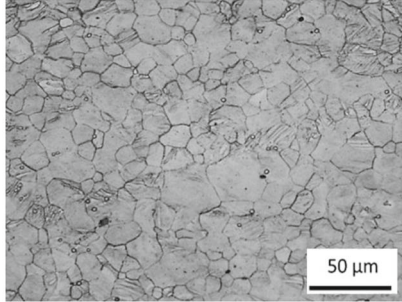
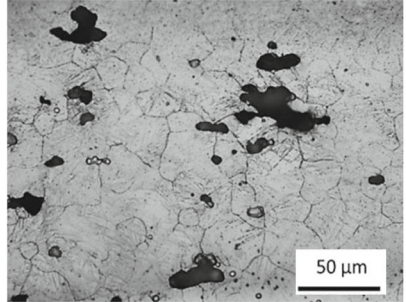
In particular, when setting the forming pressure to 723 K and 1.00 MPa, after 30 s, the mean grain size in the undeformed and in the most deformed (dome apex near the fracture) areas are  $12.3 \pm 0.5$  and  $30.8 \pm 1.8 \mu\text{m}$ , respectively. Setting the same gas pressure at 673 K, after 190 s, the mean grain size in the undeformed and in the most deformed areas are  $14.5 \pm 0.7$  and  $20.7 \pm 1.0 \mu\text{m}$ , respectively. These results denote that the static growth has a slighter effect on the grain size if compared to the dynamic growth. Results are almost consistent with the predicted ones achieved using Eq. (3) and the material constants found at 723 K by Carpenter et al. [20]: The model underestimated by a 10.4 % and by a 23.8 % the static value and the dynamic value, respectively, found in this experimentation. The relation found by Miao et al. [12] for the estimation of the static grain growth at different temperatures leads, at both 673 and 723 K, to an overestimation of the contribution of the static growth by 36.6 %. This can be related to the very short forming times that were used in the examined experiments. At the first stage of the static growth, as confirmed for lower temperatures by Yang et al., there is an incubation period of grain growth followed by a second stage of rapid grain coarsening [22]. This behaviour was related to the recrystallisation of the AZ31 alloy, even for annealed structures.

Comparing specimens in Table 3, another result is that the specimen formed at 673 K at 1.00 MPa is much more damaged in terms of cavitation than the one formed at 723 K. This difference can be attributed to the forming temperature, to the forming time and also to the strain rate difference between the specimens. Lee and Huang investigated the cavity development in an extruded AZ31 plate deformed to a strain of about 1.1 denoting that, at 673 K, the average cavity size and the cavity volume fraction are higher when setting the strain rate to  $6 \times 10^{-4} \text{ s}^{-1}$  than when setting it to  $1 \times 10^{-2} \text{ s}^{-1}$ . This can be

**Table 2** Free inflation test experimental results

Temperature, K	Pressure, MPa	Mean dome height at failure, mm	Average time to failure, s
623	0.75	21.6	2340
623	1.00	20.4	841
623	1.25	22.0	352
623	1.50	19.3	213
673	0.75	22.6	498
673	1.00	22.8	190
673	1.25	21.0	80
723	0.50	23.2	381
723	0.75	22.9	104
723	1.00	23.6	30
723	1.25	21.7	15

**Table 3** Mean grain size values and micrographs of specimens formed at 673 and 723 K with 1 MPa

temperature, K	time, s	micrograph and mean grain size in the	
		undeformed area	most deformed area
723	30		
		d = 12.3 μm	d = 30.8 μm
673	190		
		d = 14.5 μm	d = 20.7 μm

justified by the lower contribution of the GBS, that promotes cavitation at high strain rate levels [11]. Results are also in agreement with Carpenter et al. who proposed that reducing GBS creep determines a reduction of the cavitation rate [23]. An increase of cavitation was also found by Figueiredo and Langdon in an AZ31 Mg alloy processed by severe plastic deformation [24].

From these results, although the achieved final mean grain size is larger than the one achieved at lower temperatures, 723 K was chosen as the optimal working condition, since it allows not only to speed up the forming process but also to avoid, or at least to hinder, the cavitation phenomenon.

### 3.3 Calculation of strain rates in free inflation tests

The specimens formed setting the gas pressure to 1.00 MPa at both 673 and at 723 K, even if characterised by slightly different values of the dome height to failure (see Table 2), were characterised by a similar final thickness value at the dome apex: 0.17 and 0.18 mm, respectively. These correspond to an

equivalent strain of about 1.4 or to an equivalent elongation to failure of 300 %. Although the strain value at the dome apex is similar, these specimens are characterised by quite different mean grain size values in the most deformed area (see Table 3). This can be attributed to the resulting different values of the strain rate experienced by the material, calculated considering the forming times at the different temperatures. It is consistent with the results by Rabinovich and Trifonov who reported an increase, during superplastic deformation, of the grain growth rate when increasing the strain rate [25]. In the present work, the final equivalent strain at the dome apex (in which the material experiences a balanced biaxial strain state) was experimentally measured as the natural logarithm of the ratio between the initial and the final value of the thickness (about 1.4). The approximate mean strain rate value can be roughly considered inversely proportional to the forming time; in particular, considering the specimens deformed using a gas pressure of 1.00 MPa at both 673 and 723 K, they reached a strain of approximately 1.4 in 190 and 30 s, respectively (see Table 2); the related mean strain rate at the lowest

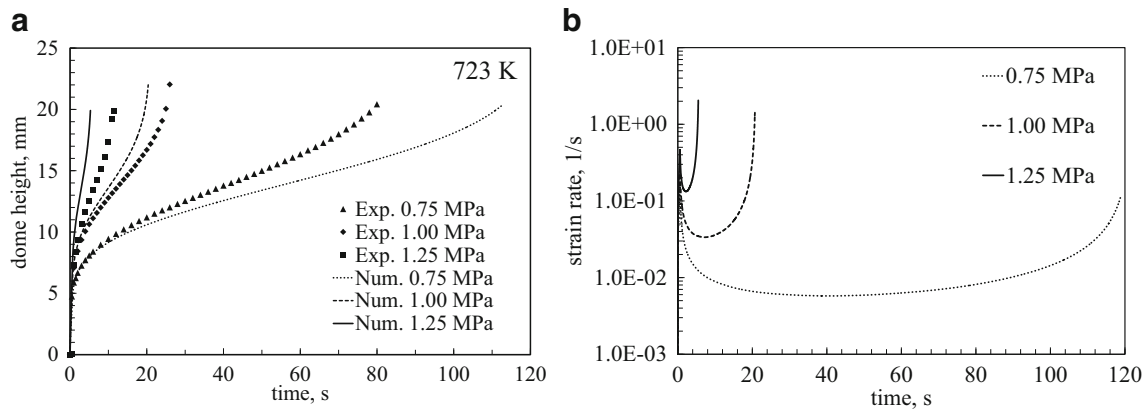


**Fig. 6** Numerical and experimental **a** dome height evolutions and **b** numerical strain rate evolution on the dome apex in free inflation tests at 723 K for three different pressure levels

temperature is thus about a sixth of the strain rate in the specimen formed at 723 K setting the gas pressure to the same level.

In Fig. 6a, the dome height versus time profiles are reported for three different pressure levels. It is thus possible to compare the numerical and experimental results at 723 K and to show the equivalent strain rate evolution during the tests conducted at the following (constant) pressure levels: 0.75, 1.00 and 1.25 MPa.

The numerical model reasonably describes the material behaviour at different pressure levels. More specifically, it can be observed that it slightly overestimates the experimental dome height values obtained setting the gas pressure at the highest level, while it underestimates the experimental values at the lowest pressure level (Fig. 6a). These discrepancies can be attributed to the grain growth model that, as previously discussed, does not perfectly catch the physical phenomenon. However, this consideration needs further investigations, and its justification goes beyond the aim of this work.

In Fig. 6b, the strain rate evolutions determined by different pressure levels have been reported as predicted by the

axisymmetric numerical model. As expected, the strain rate does not remain constant during the free inflation tests, but it has similar trends for different pressure values. The numerical mean strain rate values, calculated using Eq. (1) and according to the time paths reported in Fig. 6b (being  $t_f$  equal to the forming time to failure), were  $1.3 \times 10^{-2}$ ,  $8.4 \times 10^{-2}$  and  $2.6 \times 10^{-1} \text{ s}^{-1}$  for 0.75, 1.00 and 1.25 MPa, respectively.

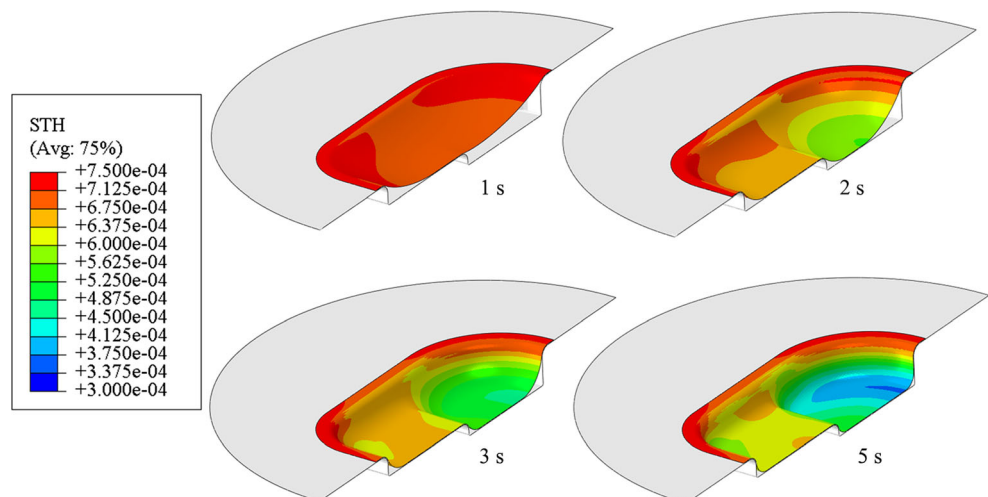
For the next step of this work, concerning the fast gas forming process analysis, the optimal value of the strain rate (at the chosen temperature of 723 K) was set to  $8.4 \times 10^{-2} \text{ s}^{-1}$ . The latter corresponds to the forming pressure value (1.00 MPa) which allowed to obtain in the free inflation tests the best compromise between formability and forming times.

## 4 Results and discussion of the closed die forming

### 4.1 Numerical analysis

Numerical simulations of the closed die forming tests were carried out setting the temperature of the blank to 723 K.

**Fig. 7** Numerical sheet thickness (STH) maps (values in meters) at four different instants of the forming process





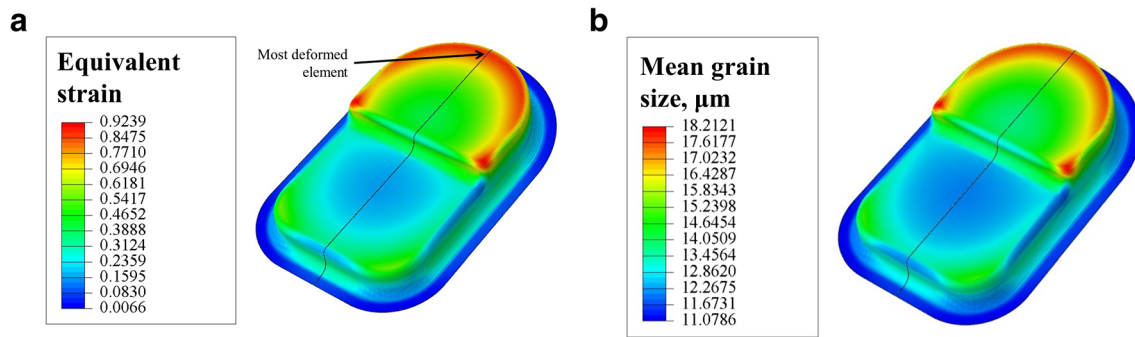


**Fig. 8** Numerical maps after 60 s with a 2.5 MPa gas pressure of **a** the equivalent creep strain and **b** of the mean grain size ( $\mu\text{m}$ )

The gas pressure was set to different levels in order to find the pressure value able to give, in the most deformed area, a mean strain rate value as close as possible to the optimal one (as found by free inflation tests). After these preliminary simulations, the attention was focused on three pressure levels: 2.00, 2.50 and 3.00 MPa. In order to understand the way the material is deformed during the process, in Fig. 7, the results from the simulation of the fast gas forming process for a given pressure of 2.50 MPa are shown in terms of sheet thickness maps at different time instants.

It can be seen that, at the beginning of the forming process, the sheet freely expands in the die cavity. Then, the sheet touches the shallowest part of the die and continues to expand in the deepest cavity: The region which experiences the largest thinning moves from the centre of the blank to the centre of the part that is still expanding. Once the sheet also touches the bottom surface of the deepest cavity, the most deformed area moves along the median axis of the cavity. Note that the thinner part of the blank is not located in the centre of the fillet radius but at its end, close to the flat region of the sheet.

In Fig. 8, results obtained by the numerical simulations of the fast gas forming process are plotted at the end of the forming process.

Comparing the strain values (Fig. 8a) and the mean grain size (Fig. 8b) maps, it can be seen that the dynamic grain growth is predominant on the static one, since the two maps are very close to each other: The most deformed areas of the blank also have the largest predicted mean grain size. Through the numerical simulations, it could be found the pressure level able to determine in the most deformed region of the blank (Fig. 8a) the mean strain rate, calculated by Eq. (1), closest to the optimal value from free inflation tests ( $8.4 \times 10^{-2} \text{ s}^{-1}$ ).

In Fig. 9, the strain rate versus the strain is plotted for the three investigated pressure levels. The strain rate of the most deformed element along the median axis (Fig. 8a) is characterised by an evolution strictly related to the case study geometry, as seen also for the strain distribution. In particular, at the beginning of the forming process, the element is free to expand in the die cavity, thus the strain rate increases. Once the sheet touches the die surface of the shallowest part of the

die cavity, also the most critical element experiences a decrease of the strain rate even if it is not in contact with the die surface yet. Then, the strain rate remains almost constant when the strain further increases, and at the end of the forming process, it drastically drops due to the contact of this element with the die surface.

In Table 4, the calculated mean strain rate values are reported. In the calculation,  $t_f$  is the time for the strain in the most deformed element to reach the value 0.9, which corresponds to an almost complete die filling.

It can be noted that the pressure level able to determine in the most deformed element a mean strain rate closest to the optimal value ( $8.4 \times 10^{-2} \text{ s}^{-1}$  from the material characterisation by free inflation tests) is 2.50 MPa.

## 4.2 Experimental forming tests

Using results from both the material characterisation and the numerical simulations, fast gas forming tests were conducted at 723 K with a constant pressure of 2.5 MPa; tests were interrupted at different forming times in order to investigate the process evolution. In Fig. 10, the results obtained by the fast gas forming tests are reported in terms of fillet radius values in the most deformed area of the case study after a

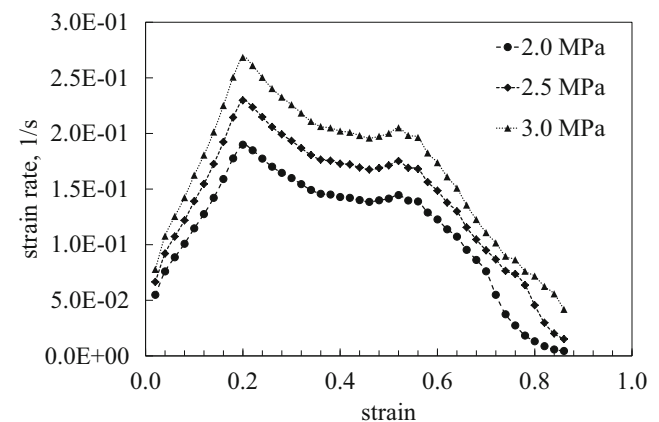


**Fig. 9** Strain rate in the most deformed element at different pressure levels plotted versus the strain value in the same element

**Table 4** Time and strain rate values of closed die forming simulations at different forming pressures

Forming gas pressure, MPa	Time to reach a strain value of 0.9, s	Mean equivalent strain rate, 1/s
2.00	22.0	$3.90 \times 10^{-2}$
2.50	10.0	$8.67 \times 10^{-2}$
3.00	7.5	$1.17 \times 10^{-1}$

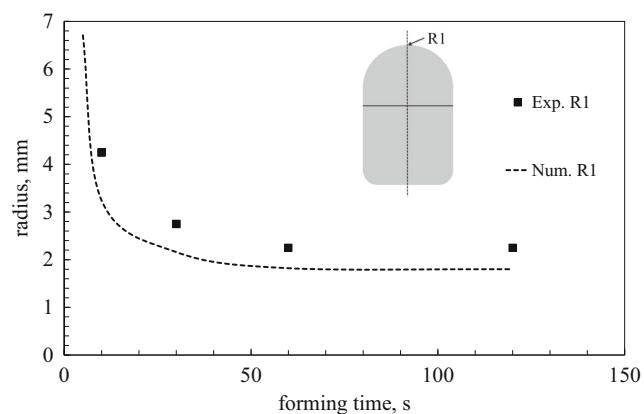
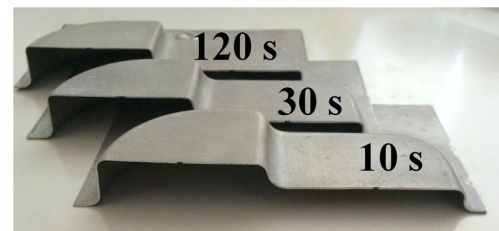
specified forming time; in the same graph, also the correspondent numerical values predicted by the FE model have been plotted.

A good agreement between the numerical results and the experimental ones is found. As expected, the fillet radius values decrease according to the forming time and a minimum value of about 2 mm was measured, thus confirming the high formability of the material at 723 K. It can be also seen that the fillet radius value rapidly decreases at the beginning of the forming process and much longer forming times are needed to achieve significantly lower values. As confirmed by the numerical simulation, the sheet touches the die in few seconds, and then, since the pressure remains constant for the whole test, the sheet slowly fills the die cavity (Fig. 11).

Since the die is filled by the deforming blank almost in the very first part of the process (after 10 s the die is almost filled) and, hereafter, the strain rate drops down to very low values, a further strong reduction of forming time can be achieved by calculating and using a pressure profile, instead of a constant value, able to keep the strain rate close to its optimal value. This approach is currently under investigation.

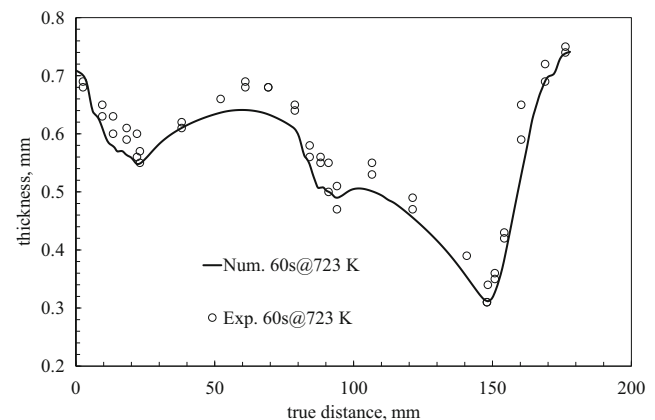
In Fig. 12, the numerical thickness distribution along the median axis of the sheet is reported together with experimental measurements.

From Fig. 12, it can be seen that experimental results are very close to numerical predictions: Errors in the thickness predictions are below the 9.4 %.

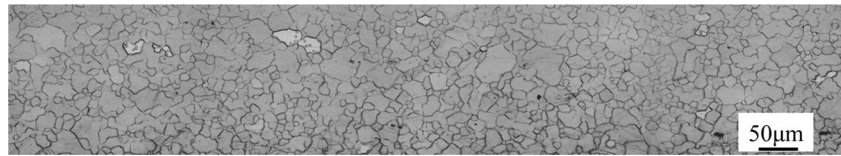
**Fig. 10** Experimental and numerical fillet radius values at 723 K under a constant pressure of 2.5 MPa at different forming times**Fig. 11** Sectioned specimens formed at 723 K with 2.5 MPa forming pressure at various forming time values

In Fig. 13, the microstructure of the alloy in the most critical area of the blank after a forming time of 60 s at 723 K is reported.

In the most critical area, the measured mean grain size value after 60 s at 723 K is  $13.2 \pm 5.3 \mu\text{m}$ . As seen by the numerical simulations, in this area, the equivalent strain reaches approximately the value of 0.92 and a not negligible dynamic grain growth is expected. The measured mean grain size at the end of the forming process, which is very close to the one in the as-received condition, indicates that the recrystallisation phenomenon (mainly dynamic since the material was purchased in the annealed condition) took part during the deformation. This is probably the reason why the numerical model (in which only the grain growth was modelled) does not perfectly match experimental results. As reported by Fatemi-Varzaneh et al., who explored the behaviour of the AZ31 Mg alloy in a similar range of temperatures and strain rates, the dynamic recrystallisation plays an important role and the percentage of recrystallised grains is strongly dependent on the temperature, on the strain rate and on the strain [26]. This result confirms that, even at 723 K, a formed component characterised by a small mean grain size (and thus by good post-forming characteristics) can be obtained. Since the grain size prediction of the numerical model shows some discrepancies with the experimental evidence, the FE model should be improved to better catch the material behaviour. More specifically, the recrystallisation phenomenon should be taken

**Fig. 12** Numerical and experimental thickness along the median axis of the formed sheet at 723 K with a gas pressure of 2.50 MPa

**Fig. 13** Microstructure of the formed sheet in the most critical area after 60 s at 723 K (forming pressure 2.5 MPa)



into account as well as the static and dynamic grain growth for the specific Mg alloy.

A not significant presence of cavities was found in the formed specimen. This is in accordance with the results of the characterisation by free inflation tests. As also stated by Lee and Huang, the cavity volume fraction increases more than linearly with the strain and it follows an approximately exponential law with the strain, especially for low strain rate values [11]. Considering that, during the free inflation tests, the alloy reaches a strain of about 1.4 (see Sect. 3.3), a relative small quantity of cavities at 673 K should also be expected in the closed die fast gas forming tests due to the lower strain value experienced by the blank (the equivalent strain value in the most critical area of the blank is about 0.9, far below the maximum equivalent strain that the material achieved in free inflation tests). This statement should be experimentally verified also considering that at 673 K, the forming time would be much higher than the one found at 723 K and estimating the effective saving in terms of the energy costs.

An additional aspect which should be taken into account is the final surface roughness. In fact, it can be, especially in aesthetic applications, as important as post-forming mechanical properties. Increasing the temperature strongly reduces the forming time, but a worse surface finishing is probably achieved due to the higher temperature level. This aspect needs further investigations focusing the attention on the surface quality, thus considering the roughness of the component surfaces as an output value of the forming process.

## 5 Conclusions

In this work, both inflation tests and closed die forming tests were carried out on an AZ31 magnesium alloy, being the main aim to explore the fast gas forming process potentialities. Through the analysis of experimental and numerical results, the following conclusions can be drawn:

- When operating at high pressure levels, a process window characterised by a good formability together with short forming times can be found at both 673 and 723 K;
- Even if the alloy is prone to a strong static grain growth, the dynamic growth is predominant due to the short forming times;
- In the process window characterised by a good formability and short forming times, the cavitation phenomenon

can be hindered operating at 723 K and at higher strain rates;

- Very small fillet radius values (2 mm) can be achieved after a forming time of 60 s;
- The operating temperature of 723 K represents a valuable compromise between forming times, microstructure and formability: Due to the short forming times, a formed component with small mean grain size can be obtained even at a temperature level in which the static growth is severe (723 K) for the AZ31 Mg alloy.

**Acknowledgments** The authors wish to thank the Italian Institutions Region APULIA and MIUR (Ministry of Education, University and Research) for financing the present research activity (TRASFORMA and PRIN BIOFORM projects). The authors are also grateful to Dr. R. Di Mundo and to Dr. C. Annese for their help in the metallographic observations.

## References

1. Neugebauer R, Altan T, Geiger M, Kleiner M, Sterzing A (2006) Sheet metal forming at elevated temperatures. *Ann CIRP* 55(2): 793–816
2. Lee S, Chen Y-H, Wang J-Y (2002) Isothermal sheet formability of magnesium alloy AZ31 and AZ61. *J Mater Process Technol* 124: 19–24
3. Boissière R, Blandin JJ, Salvo L (2010) Large deformability of wrought magnesium alloys: is superplasticity needed? *Key Eng Mater* 433:267–272
4. Krajewski PE, Schroth JG (2007) Overview of quick plastic forming technology. *Mater Sci Forum* 551–552:3–12
5. Sun P-H, Wub H-Y, Tsaib H-H, Huang C-C, Tzoub M-D (2010) Effect of pressurization profile on the deformation characteristics of fine-grained AZ31B Mg alloy sheet during gas blow forming. *J Mater Process Technol* 210:1673–1679
6. Zhang D-T, Xiong F, Zhang W-W, Qiu C, Zhang W (2011) Superplasticity of AZ31 magnesium alloy prepared by friction stir processing. *Trans Nonferrous Metals Soc China* 21:1911–1916
7. Chung SW, Higashi K, Kim WJ (2004) Superplastic gas pressure forming of fine-grained AZ61 magnesium alloy sheet. *Mater Sci Eng A* 372:15–20
8. Wu H-Y, Sun P-H, Zhu F-J, Liu H-C, Chiu C-H (2012) Tensile properties and shallow pan rapid gas blow forming of commercial fine-grained Mg alloy AZ31B thin sheet. *Procedia Eng* 36:329–334
9. El-Morsy A-W, Manabe K-I, Nishimura H (2002) Superplastic forming of AZ31 magnesium alloy sheet into a rectangular pan. *Mater Trans* 43–10:2443–2448
10. Kim W-J, Chung SW, Chung CS, Kum D (2001) Superplasticity in thin magnesium alloy sheets and deformation mechanism maps for magnesium alloys at elevated temperatures. *Acta Mater* 49–16: 3337–3345
11. Lee CJ, Huang JC (2004) Cavitation characteristics in AZ31 Mg alloys during LTSP or HSRSP. *Acta Mater* 52:3111–3122

12. Miao Q, Hu L, Wang X, Wang E (2010) Grain growth kinetics of a fine-grained AZ31 magnesium alloy produced by hot rolling. *J Alloys Compd* 493:87–90
13. Sorgente D, Scintilla LD, Palumbo G, Tricarico L (2010) Blow forming of AZ31 magnesium alloy at elevated temperatures. *Int J Mater Form* 3:13–19
14. Hosokawa H, Chino Y, Shimojima K, Yamada Y, Wen C, Mabuchi M, Iwasaki H (2003) Mechanical properties and blow forming of rolled AZ31 Mg alloy sheet. *Mater Trans* 44–4:484–489
15. Verma R, Hector LG, Krajewski PE, Taleff EM (2009) The finite element simulation of high-temperature magnesium AZ31 sheet forming. *JOM* 61–8:29–37
16. Carter JT, Krajewski PE, Verma R (2008) The hot blow forming of AZ31 Mg sheet: formability assessment and application development. *JOM* 60–11:77–81
17. Sorgente D, Tricarico L (2014) Characterization of a superplastic aluminium alloy ALNOVI-U through free inflation tests and inverse analysis. *Int J Mater Form* 7:179–187
18. Abaqus 6.10 online documentation, 2010, © dassault systèmes
19. Hanna MD (2009) Tribological evaluation of aluminum and magnesium sheet forming at high temperatures. *Wear* 267:1046–1050
20. Carpenter AJ, Antoniswamy AR, Carter JT, Hector LG Jr, Taleff EM (2014) A mechanism-dependent material model for the effects of grain growth and anisotropy on plastic deformation of magnesium alloy AZ31 sheet at 450°C. *Acta Mater* 68:254–266
21. Sato E, Kuribayashi K, Horiuchi R (1988) Grain growth induced by superplastic deformation in Zn-22% Al alloy. *Nippon Kinzoku Gakkai-si* 52–11:1043–1050
22. Yang X-Y, Zhu Y-K, Miura H, Sakai T (2010) Static recrystallization behavior of hot-deformed magnesium alloy AZ31 during isothermal annealing. *Trans Nonferrous Metals Soc China* 20:1269–1274
23. Carpenter AJ, Carter JT, Hector Jr, LG, Taleff EM (2013) Gas-pressure bulge forming of Mg AZ31 sheet at 450°C. In: Hort N, Mathaudhu SN, Neelameggham NR, Alderman M (eds), *Magnesium technology 2013*. TMS (The Minerals, Metals & Materials Society), pp. 139–144
24. Figueiredo RB, Langdon TG (2012) Influence of rolling direction on flow and cavitation in a superplastic Magnesium alloy processed by equal-channel angular pressing. *Mater Sci Eng A* 556:211–220
25. Rabinovich MK, Trifonov VG (1996) Dynamic grain growth during superplastic deformation. *Acta Mater* 44–5:2073–2078
26. Fatemi-Varzaneh SM, Zarei-Hanzaki A, Beladi H (2007) Dynamic recrystallization in AZ31 magnesium alloy. *Mater Sci Eng A* 456: 52–57